Journal of Power Sources 195 (2010) 5013–5018

Contents lists available at ScienceDirect

Journal of Power Sources

journal homepage: www.elsevier.com/locate/jpowsour

Synthesis and characterization of $Li_3V_{(2-2x/3)}Mg_x(PO_4)_3$/C cathode material for lithium-ion batteries

J.S. Huang, L. Yang*, K.Y. Liu, Y.F. Tang

School of Chemistry and Chemical Engineering, Shanghai Jiao Tong University, Shanghai 200240, PR China

ARTICLE INFO

Article history:
Received 4 November 2009
Received in revised form 27 January 2010
Accepted 4 February 2010
Available online 10 February 2010

Keywords:
Lithium-ion battery
$Li_3V_2(PO_4)_3$
Mg-doping
Sol–gel assisted

ABSTRACT

$Li_3V_{(2-2x/3)}Mg_x(PO_4)_3$/C ($x$ = 0, 0.15, 0.30, 0.45) composites have been synthesized by the sol–gel assisted solid state method, using adipic acid $C_6H_{10}O_4$ (hexanedioic acid) as carbon source. The particle size of the composites is ~1 μm. During the pyrolysis process, $Li_3V_{(2-2x/3)}Mg_x(PO_4)_3$/C network structure is formed. The effect of Mg^{2+} doped on the electrochemical properties of $Li_3V_2(PO_4)_3$/C positive materials has been studied. $Li_3V_{1.8}Mg_{0.30}(PO_4)_3$/C as the cathode materials of Li-ion batteries, the retention rate of discharge capacity is 91.4% (1 C) after 100 cycles. Compared with $Li_3V_2(PO_4)_3$/C, $Li_3V_{(2-2x/3)}Mg_x(PO_4)_3$/C composites have shown enhanced capacity and retention rate capability. The long-term cycles and ex situ XRD tests disclose that $Li_3V_{1.8}Mg_{0.30}(PO_4)_3$ exhibits higher structural stability than the undoped system.

1. Introduction

Phosphate polyanion framework materials are being considered as favorable replacements for oxide-based materials as the cathode materials in lithium battery applications. In this regard, the $LiMPO_4$ (M = Fe, Co, Ni, Mn) [1–5], and $Li_3V_2(PO_4)_3$ [6–12] have all shown considerable promise. They contain both mobile Li ions and redox-active metals within a rigid phosphate network, displaying remarkable electrochemical and stability. Among these, the $Li_3V_2(PO_4)_3$ is highly promising materials proposed as a cathode for high voltage lithium-ion batteries because it possesses high reversible capacity, high operate voltage, good ion mobility [7,9,13], and so on.

Unfortunately, the capacity and rate performance of polyanion materials strongly depend on their electronic conductivity (only in the lever of 10^{-10} to 10^{-9} S cm^{-1} for pure $LiFePO_4$ [14] and 10^{-8} to 10^{-7} S cm^{-1} for $Li_3V_2(PO_4)_3$ [9,15]). It has been proved that metal doping or mixing with electrically conductive materials such as carbon could effectively improve electronic conductivity of $Li_3V_2(PO_4)_3$ [10]. The Zr-doped $Li_3V_2(PO_4)_3$ [16] exhibited not only the enhancement of the discharge capacity but also disappearance of the two-plateau boundary in the charge/discharge curves. The results showed that the ionic conductivity of Ti-doped $Li_3V_2(PO_4)_3$ [17] was increased to three orders of magnitudes, and the specific capacity was improved, and the two-plateau boundary in the charge–discharge curves was disappeared. In the $Li_3Fe_xV_{2-x}(PO_4)_3$ system [18], all the Fe-doped samples exhibited higher discharge capacity than the undoped samples. The results of $Li_3V_{2-x}Al_x(PO_4)_3$ [19] suggested that the substituted phases encouraged performance with high material utilization and comparatively low discharge-capacity fading. In $Li_3V_{2-x}Cr_x(PO_4)_3$/C composite [20], both cycle performance and rate capability have been improved obviously.

The doping in V sites by Co^{2+} was favorable for the structural stability of $Li_3V_{2-x}Co_x(PO_4)_3$/C [21] compounds and thus counteracted the volume changes during the reversible Li^+ extraction/insertion, resulting in improved cycling ability. Mg^{2+} doping has been proved effectively to improve ionic conduct of $LiFePO_4$ and enhance the capacity and the rate capability, without olivine structure changes [22,23]. On the other hand, the replacement of V^{3+} with Mg^{2+} is considered favorable due to that the atomic weight of Mg is lighter than the V. In this paper, Mg^{2+} doped $Li_3V_2(PO_4)_3$ was prepared by an adipic acid-assisted simple sol–gel method. The pyrolysis of hexanedioic acid not only prevented the agglomeration of small particles, but also provided vigorous reduction atmosphere and changed to uniform residue carbon network. It was proved that Mg^{2+} incorporation in $Li_3V_2(PO_4)_3$ could allow the formation of active phases which exhibited beneficial electrochemical properties, including enhanced specific capacity and good cycle-life performance. In $Li_3V_{1.8}Mg_{0.30}(PO_4)_3$/C phase, the retention rate of discharge capacity is 91.4% (1 C) after 100 cycles. The $Li_3V_{1.8}Mg_{0.30}(PO_4)_3$/C presents higher structure stability than the undoped system.

* Corresponding author.
E-mail address: liyangce@sjtu.edu.cn (L. Yang).

0378-7753/$ – see front matter © 2010 Elsevier B.V. All rights reserved.
doi:10.1016/j.jpowsour.2010.02.009

2. Experimental

2.1. Preparation of $Li_3V_{(2-2x/3)}Mg_x(PO_4)_3$/C composites

The $Li_3V_{(2-2x/3)}Mg_x(PO_4)_3$/C ($x$ = 0.00, 0.15, 0.30 and 0.45) composites were synthesized as follow. Hexanedioic acid ($C_6H_{10}O_4$) was used here not only as a chelating regent but also as carbon sources. Oxalic acid and V_2O_5 in a stoichiometric ratio (3:1) were dissolved in deionized water with magnetic stirring at 70 °C [10]. After a clear blue solution obtained, a mixture of stoichiometric $NH_4H_2PO_4$, Li_2CO_3, $Mg(CH_3COO)_2$ and $C_6H_{10}O_4$ was added to the solution, while stirring for 4 h, then a gel was formed in an air oven at 100 °C. The gel was initially heated to 350 °C in N_2 atmosphere for 4 h to allow H_2O and NH_3. The resulting product was heated to 750 °C for 4 h in flowing N_2. All the reagents used in the experiment were analytical purity and purchased from Sinopharm Chemical Reagent Co., Ltd (SCRC), and used without further purification.

2.2. Sample characterization

The structure and morphology of the products were characterized by X-ray diffraction measurement (XRD, Rigaku, D/max-RBusing Cu Kα radiation with λ = 1.5418 Å) and field emitting scanning electron microscopy (FESEM, JEOL JSM-7401F). After cycling, the cells were carefully opened in a glove box to recover the electrode, and the electrodes were subsequently rinsed in diethyl carbonate (DEC) to remove the residual $LiPF_6$ and dried at 80 °C. The dried electrodes were subjected to ex situ XRD in order to evaluate any structural changes. The carbon content was verified by thermogravimetrics analysis coupled with element analysis.

2.3. Electrochemistry measurement

Coin-type half-cell tests were conducted on samples that had different C (1 C = 140 mAh g^{-1}) rates in the range of 3.0–4.5 V, and the same charge and discharge rates were used. For electrochemical testing, composite electrodes were fabricated using 80 wt% active materials, 10 wt% carbon (containing residue carbon in the synthesized active material and carbon black added to the electrode in fabrication of electrode), and 10 wt% polylvinylidene fluoride (PVdF). The active material loading for the cathode was in the range of 5–6 mg cm^{-2}.

The coin-type battery test cells (size 2016R), each of which contained a cathode, a Li metal anode, and glass fiber filter (Whatman, GF/A) as separator, were prepared in a argon-filled glove box (German, M. Braun Co., [O_2] < 1 ppm, [H_2O] < 1 ppm). The electrolyte used was 1 M $LiPF_6$ with EC/DEC/EMC (1/1/1 vol%).

A CHI604b electrochemical workstation was used for cyclic voltammetry measurements. Complex impedance measurements were carried out using a CHI604b impedance analyzer in the frequency range 10^{-2} to 10^5 Hz. The galvanostatic charge/discharge tests were performed with a Land CT2001 battery tester at 25 °C.

3. Results and discussions

3.1. Sample characterization

Fig. 1 depicts the raw XRD powder patterns obtained for the various Mg^{2+} contents $Li_3V_{(2-2x/3)}Mg_x(PO_4)_3$/C composites. The samples (x = 0, x = 0.15, x = 0.30) were identified to be $Li_3V_2(PO_4)_3$ phase monoclinic (space group $P2_1/n$) with no unwanted impurities [9,17]. Trace impurity was found in sample (x = 0.45). Table 1 showed the cell parameter of $Li_3V_{(2-2x/3)}Mg_x(PO_4)_3$/C, and it can be seen that the parameter of cell unit decreases after the Mg^{2+} doping. During the heating process, the soft amorphous hydrocarbon may be formed in the range of 400–600 °C, but it was transformed into hard carbon at high temperature (up to 600 °C) [24,25]. The carbon content in the $Li_3V_{(2-2x/3)}Mg_x(PO_4)_3$/C composite was validated by thermogravimetric analysis and element analysis. The residue carbon contents of $Li_3V_2(PO_4)_3$/C and $Li_3V_{1.8}Mg_{0.30}(PO_4)_3$/C are 2.8% and 4.4%, respectively.

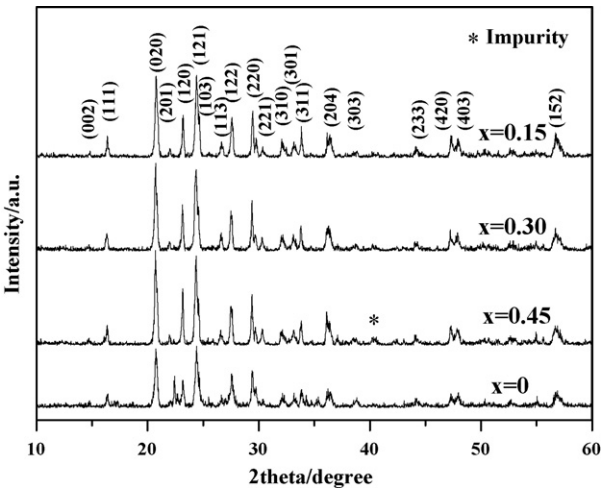

Fig. 1. Typical XRD patterns of $Li_3V_{(2-2x/3)}Mg_x(PO_4)_3$/C with x = 0, 0.15, 0.30, 0.45.

Fig. 2 shows the SEM images of the synthesized $Li_3V_{(2-2x/3)}Mg_x(PO_4)_3$/C samples. It can be seen that the particles of the sample merge with each other and form a porous network. With the heating temperature increases, the pyrolysis carbon becomes to act as the chelating agent to bridge amorphous $Li_3V_2(PO_4)_3$ for formation of the $Li_3V_{(2-2x/3)}Mg_x(PO_4)_3$/C composite network. This geometry has several advantages such as good accommodation of volume changes without fracture during cycling, good electrical connection with the current collector and efficient for electron transportation. This microstructure is beneficial for the electrolyte to penetrate with the positive materials, which is promoted for good electronic contact among the composites particles.

3.2. Galvanostatic electrochemical measurements.

The initial charge/discharge curves are shown in Fig. 3 for the test cells at 0.2 C charge/discharge rate in the range of 3.0–4.5 V at room temperature. The charge curves of the four samples are almost the same. On charge, voltage plateaus at around 3.6 V vs Li and 4.1 V vs Li are associated with the extraction of the first two Li ions, but the discharge plateau is a little longer in the discharge curve of the Mg-doped $Li_3V_2(PO_4)_3$ than the undoped sample. By comparison, the V^{3+} activity $Li_3V_{(2-2x/3)}Mg_x(PO_4)_3$/C is changed due to the presence of the inactive Mg^{2+}, so the plateau is diminishing with increased Mg^{2+} content (x = 0.45). The significant effects are observed from the long-term charge/discharge cyclic performances in the following tests, as shown in Fig. 4.

Fig. 4 demonstrates the preliminary life cycle performance for a larger range of the Mg^{2+} substituted phases $Li_3V_{(2-2x/3)}Mg_x(PO_4)_3$/C, all the Mg-doped samples exhibit

Table 1
Unit cell parameters of $Li_3V_{(2-2x/3)}Mg_x(PO_4)_3$/C (where x = 0.00, 0.15, 0.30, 0.45).

Samples (×value)	a (Å)	b (Å)	c (Å)	β (°)	V (Å^3)
0.00	8.608(3)	8.553(6)	12.060(3)	90.363(5)	888.0(2)
0.15	8.591(7)	8.501(3)	12.106(7)	90.525(2)	884.2(4)
0.30	8.499(5)	8.533(5)	12.137(2)	90.357(7)	880.3(1)
0.45	8.584(5)	8.515(7)	12.127(7)	90.697(7)	886.5(1)

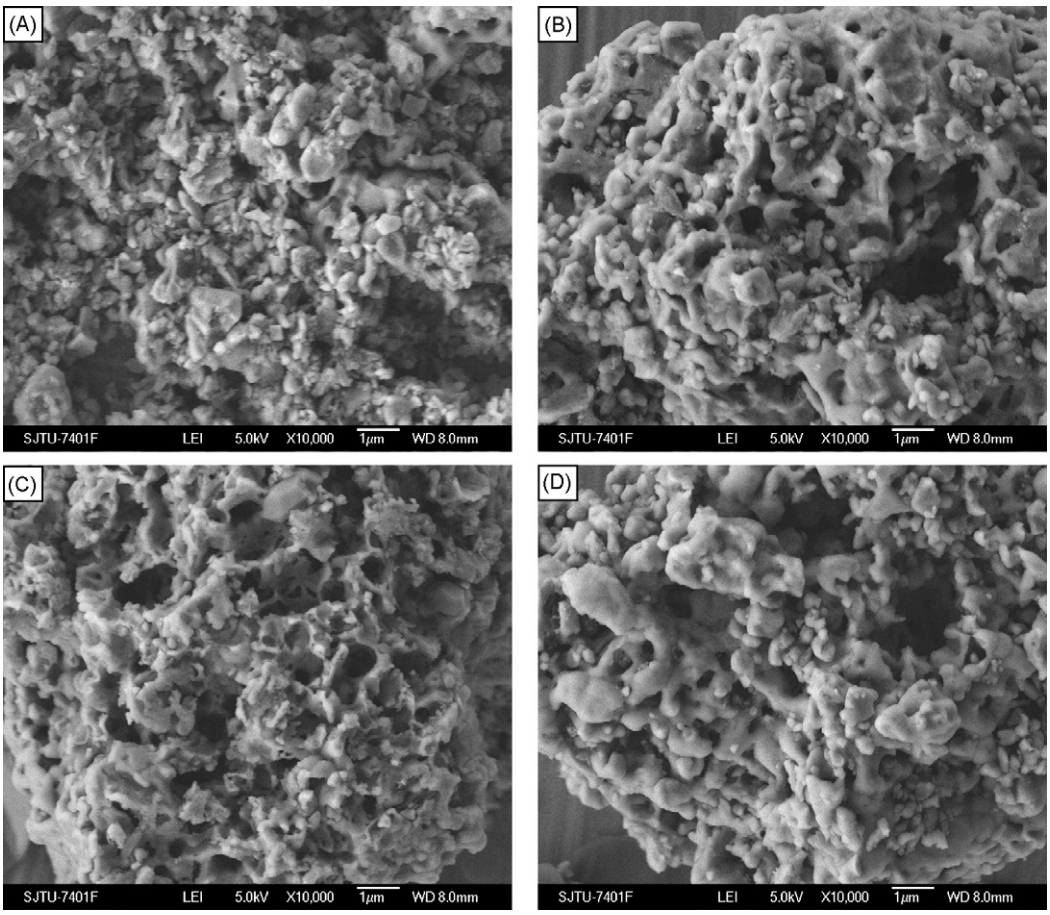

Fig. 2. SEM images of $Li_3V_{(2-2x/3)}Mg_x(PO_4)_3/C$ with $x = 0$ (a), 0.45 (b), 0.30 (c), 0.15 (d).

higher discharge specific capacity than the undoped samples, meaning that Mg-doped samples have better cyclic ability and electrochemical stability. Where $x = 0.30$, the discharge capacity is larger than the other contents. The discharge capacity of $Li_3V_{1.8}Mg_{0.30}(PO_4)_3/C$ is 118 mAh g^{-1} at 0.2C after 100 cycles, much higher than the undoped $Li_3V_2(PO_4)_3/C$ (79.8 mAh g^{-1} after 87 cycles), so the retention rate in the discharge capacities is 92.2% after 100 cycles, but only 86.6% for pure $Li_3V_2(PO_4)_3/C$. At higher current density (1 C rate), the retention rate in discharge of $Li_3V_{1.8}Mg_{0.30}(PO_4)_3/C$ still keeps at 91.4%. The results display

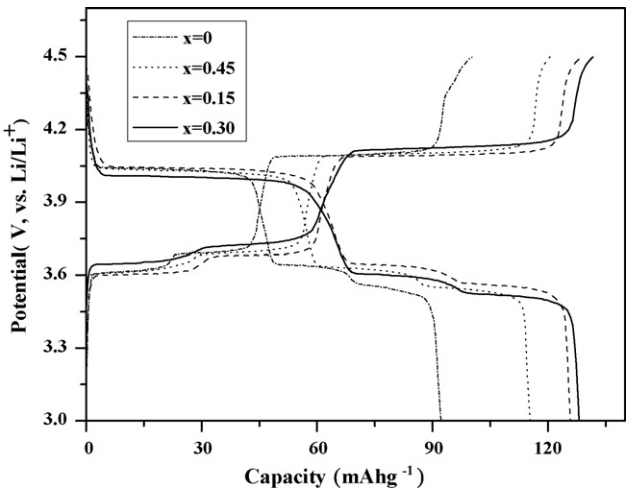

Fig. 3. Typical charge/discharge curves of $Li_3V_{(2-2x/3)}Mg_x(PO_4)_3/C$ at 0.2 C.

that doping with small amount of Mg^{2+} is resulted in good cycling stability and large discharge capacity. Both low Mg^{2+} content $x = 0.15$ and high Mg^{2+} content $x = 0.45$ has enhanced capacity of the $Li_3V_2(PO_4)_3$ cathode materials during cycling, but the retention rates are not as well as the optimal $x = 0.30$ sample. It is easy to understand that too small amount of Mg^{2+} doping only gives slight effect on the crystal structure, but the existence of too many Mg^{2+} ions in the crystal lattice may induce large changes to the structure and cause the phase instability. Meanwhile, the Mg^{2+} is electrochemical inactive under this condition. This means that overmuch Mg^{2+} ions reduce the utilization of active cathode materials. Therefore, the optimal Mg^{2+} content x is 0.30 in this investigation. The $Li_3V_{1.8}Mg_{0.30}(PO_4)_3/C$ sample will be taken as an example in the following measurements.

3.3. Differential capacity profile

The differential capacity curves are shown in Fig. 5 for $x = 0$ and $x = 0.30$ samples. The three oxidation peaks (C_1, C_2, C_3) are located around 3.70, 3.80, and 4.20 V. The corresponding lithium insertion reaction are denoted as peaks D_1 through D_3. The voltage peaks associated with $Li_3V_{1.8}Mg_{0.30}(PO_4)_3$ has shifted to lower voltage about 0.5 V compared to the undoped sample, in agreement with the charge/discharge curves (Fig. 3). Note the relatively broad differential capacity curves which dominate the discharge process and correspond to the relatively smooth discharge voltage profile [19]. The observation may prove significant from a commercial viewpoint because it means that a relatively little addition of Mg^{2+} allows the user to fully utilize the active material at a lower charge voltage. This may facilitate good long-term performance because

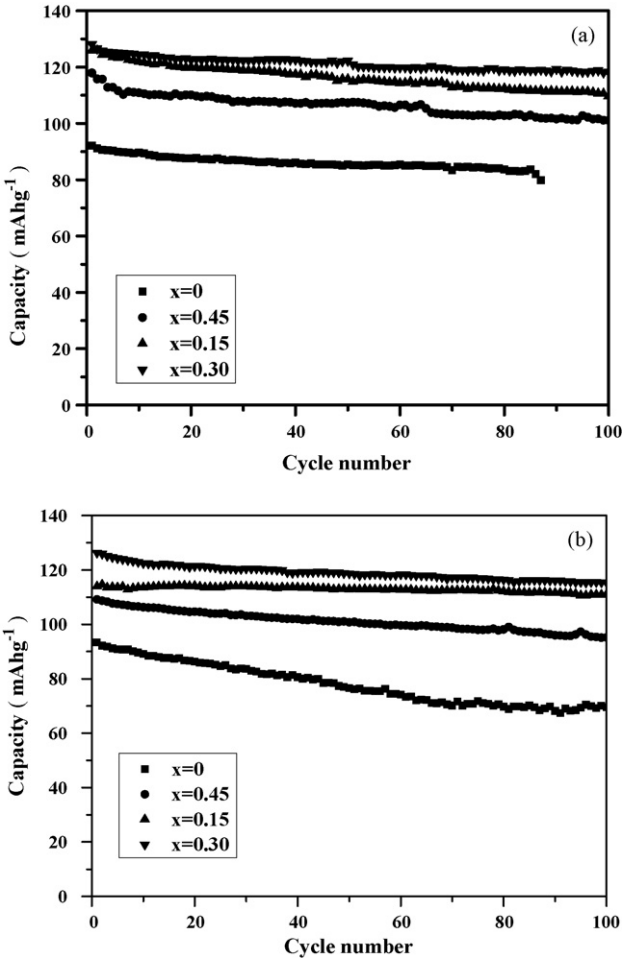

Fig. 4. Cycle performance comparisons of $Li_3V_{(2-2x/3)}Mg_x(PO_4)_3$/C with $x = 0$, 0.15, 0.30, 0.45 at various charge–discharge rates at room temperature: (a) 0.2 C, (b) 1 C.

the electrochemical stability window of the electrolyte can be seriously compromised at such high oxidative voltages.

3.4. EIS analysis

To further understand the electrochemical behavior of $Li_3V_{(2-2x/3)}Mg_x(PO_4)_3$, Electrochemical impedance spectroscopy (EIS) was used to study the electrode kinetics of different samples. Fig. 6(a) shows the EIS of the positive electrodes for the samples in the first charge cycle. Both electrodes exhibit a semicircle in the high-frequency range and an inclined line in the low frequency range. The high-frequency semicircle is assisted to the charge-transfer impendence in the electrode and electrolyte interface, and the inclined line corresponds to the lithium-ion diffusion process. The diameter of semicircle on the sample ($x = 0.30$) is obviously smaller than that of the sample ($x = 0$), which implies that the insertion/extraction of Li^+ ions is facile in $Li_3V_{1.8}Mg_{0.30}(PO_4)_3$/C sample.

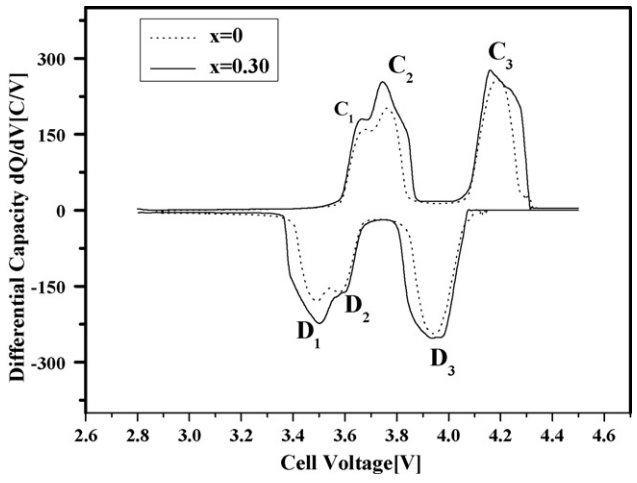

Fig. 5. Differential capacity curves of $Li_3V_2(PO_4)_3$/C and $Li_3V_{1.8}Mg_{0.30}(PO_4)_3$/C record in 3–4.5 V for the second cycle.

Fig. 6(b) shows the EIS $Li_3V_{1.8}Mg_{0.30}(PO_4)_3$ of the in the first charge cycle. The tests were carried out at various voltages in the range of 3.6-4.4 V. The data were analyzed by fitting to an equivalent electrical circuit shown in Fig. 7 [26,27]. Fig. 7 consisting resistance (R_i), R_i||CPE_i combinations, R_e, $R_{(sf+ct)}$, and R_b are impedances (resistances) due to electrolyte and cell components, surface film (sf) plus charge transfer (ct) and bulk (b), respectively. CPE_i is the respective constant phase element to account for the depressed semicircle in the experimental spectra (dl refers to double layer). W_s is the finite length Warburg (short circuit terminus) element and an intercalation capacitance (C_{int}). In Fig. 6, only one semicircle is seen in the high-to-medium-frequency range indicating that effects due to sf and ct are not separable. In this case, a proper assignment will be $R_{(sf+ct)}$ and $CPE_{(sf+dl)}$. The contribution to R_b comes not only from the bulk impedance of the active materials, but also from the electrolyte trapped in the pores of the composite electrode and that due to the inhomogeneous coating of active material on the current collector.

Fig. 8 shows the plots of $R_{(sf+ct)}$ versus voltage. The lines jointing the data point are only a guide to the eye. It can be seen that the $R_{(sf+ct)}$ of the $Li_3V_{1.8}Mg_{0.30}(PO_4)_3$/C decreases rapidly initially and then keeps relatively stability. $R_{(sf+ct)}$ may play an influential role in the electrode kinetics of samples, it will effect the electrochemical performance. So the Mg^{2+} undoped $Li_3V_2(PO_4)_3$/C has unsatisfactory electrochemical performance.

3.5. Ex situ XRD patterns after long-term cycles

The XRD patterns of the $x = 0.30$ (a) and $x = 0$ (b) samples after 100 charge/discharge cycles at 1 C are presented in Fig. 9. It shows a similar XRD pattern to that of the original $Li_3V_{1.8}Mg_{0.30}(PO_4)_3$ phase in Fig. 1. This result indicates that the original monoclinic phase could be recovered even after many charge/discharge cycles, and only the XRD peaks become broader, which the usual phenomena is resulting from the pulverization of active materials during long-term cycles [28]. Therefore, it is possible that the existence of Mg^{2+} ions could counteract the volume shrinking/swelling during the Li^+ reversible extraction/insertion and enhance the stability in the charge and discharge cycles. The expansion in the crystal lattice could allow more space for lithium insertion and de-insertion. During the de-insertion process, the lattice would be prevented from shrinking by the Mg^{2+} dopant ions, which is due to the unchangeable radius of Mg^{2+}. It has been reported that the phase stability of orthorhombic was enhanced by Zr^{4+} [16] and Fe^{3+} [18] doping. On the other hand, the existence of Mg^{2+} will cause some local defects in the crystal structure, leading to the increase of electrical conductivity and ionic diffusion, so the cyclic performance of the system are remarkably improved through the doping of small amount of Mg^{2+}. In the case of V^{3+}, it will be changed to V^{4+}, V^{5+} during de-insertion, which is smaller. As a result, the lattice will collapse and limit diffusion of lithium ions. In the $x = 0.30$ sample, Mg^{2+} in the lattice could act as a pillar to prevent the collapse of the crystal during cycling, as hetero-atoms doping in $LiMn_2O_4$ [29,30].

But large amount Mg^{2+} ($x = 0.45$) may induce large changes to the structure and cause the phase instability. Further investigation

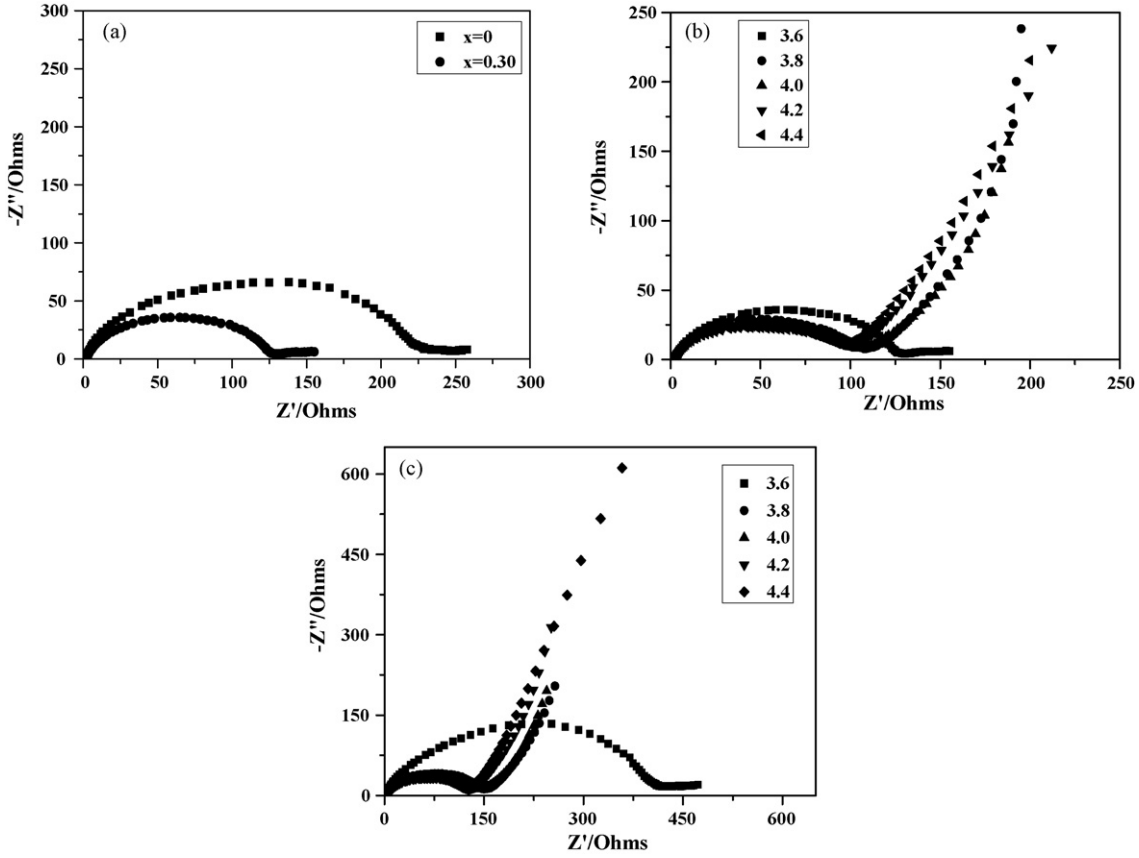

Fig. 6. Nyquist plots of $Li_3V_2(PO_4)_3$/C and $Li_3V_{1.8}Mg_{0.30}(PO_4)_3$/C electrodes measured at the charge potential of 3.6 V during the first cycle (a), Impedance spectra of $Li_3V_{1.8}Mg_{0.30}(PO_4)_3$/C and $Li_3V_2(PO_4)_3$/C at different voltages during the first charging operation (b and c).

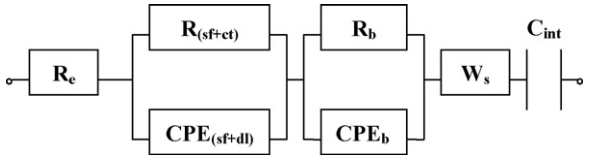

Fig. 7. Equivalent circuit used for fitting the impedance spectra of Fig. 6(b and c).

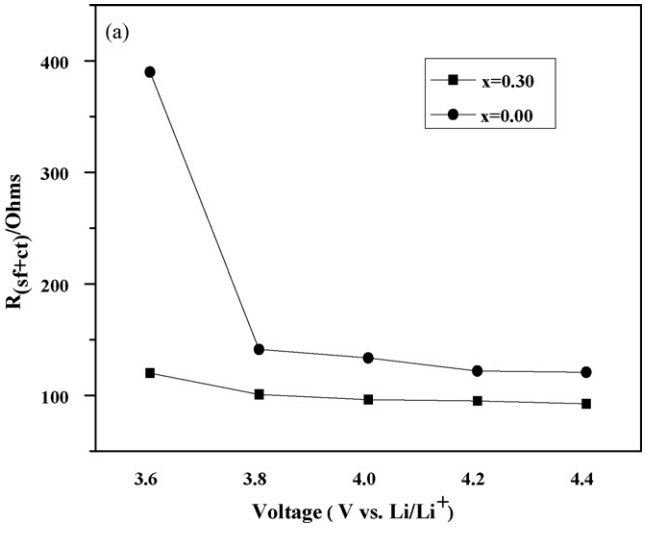

Fig. 8. Variation of surface film + charge-transfer resistance ($R_{(sf+ct)}$) as a function of voltage during the 1st charge cycle.

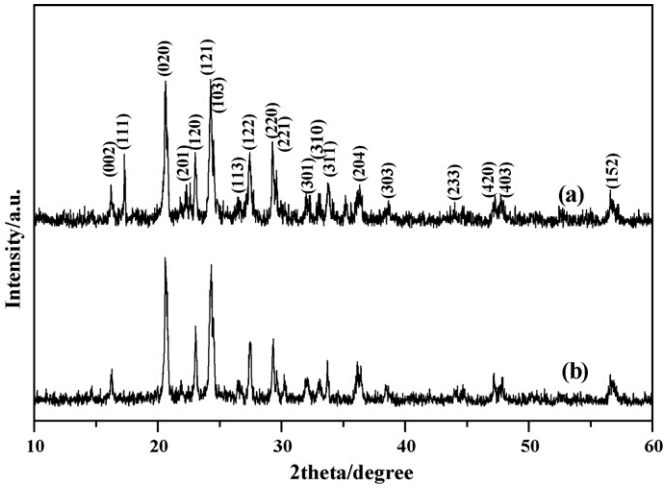

Fig. 9. Ex situ XRD pattern of (a) $Li_3V_2(PO_4)_3$/C and (b) $Li_3V_{1.8}Mg_{0.30}(PO_4)_3$/C after 100 charge/discharge cycles at 1 C.

are still necessary to completely clarify the Mg^{2+} doping effects on the $Li_3V_2(PO_4)_3$.

4. Conclusions

In this work, the various Mg^{2+} contents $Li_3V_{(2-2x/3)}Mg_x(PO_4)_3$/C cathode materials were synthesized by sol–gel assisted solid state method. XRD indicated that a monoclinic phase (14($P2_1/n$)) was obtained. Using adipic acid (hexanedioic acid) as carbon source, the carbon was formed slowly under pyrolysis, and it was more

beneficial to form network structure of $Li_3V_{(2-2x/3)}Mg_x(PO_4)_3$/C. Electrochemical tests indicate that the Mg-doped $Li_3V_2(PO_4)_3$ samples have good charge/discharge cyclic stability. The optimal Mg-doping content x is 0.30 in $Li_3V_{(2-2x/3)}Mg_x(PO_4)_3$/C, which have the highest discharge capacity and good cyclic stability. According to the ex situ XRD after long-term cycles, the structure stability of $Li_3V_{1.8}Mg_{0.30}(PO_4)_3$ is enhanced by the Mg-doping, which is higher than the undoped system. In $Li_3V_{1.8}Mg_{0.30}(PO_4)_3$/C composite, the retention rate of discharge capacity is 91.4% (1 C) after 100 cycles. However, the undoped $Li_3V_2(PO_4)_3$/C shows a fast decline in capacity during the cycling and has 25.6% capacity fading of the initial value after 100 cycles. It indicates that the $Li_3V_{(2-2x/3)}Mg_x(PO_4)_3$/C prepared by hexanedioic acid sol–gel assisted solid state method has enhanced electrochemical performance and structural stability.

Acknowledgements

The authors are indebted to the National Key Project of China for Basic Research under grant no. 2006CB202600 and the National High Technology Research and Development Program of China under grant no. 2007AA03Z222. We thank the Instrumental Analysis Center of Shanghai Jiao Tong University for Materials Characterization.

References

[1] A.K. Padhi, K.S. Nanjundaswamy, J.B. Goodenough, J. Electrochem. Soc. 144 (1997) 1188–1194.
[2] J.J. Chen, S.J. Wang, M.S. Whittingham, J. Power Sources 174 (2007) 442–448.
[3] H.H. Li, J. Jin, J.P. Wei, Z. Zhou, J. Yan, Electrochem. Commun. 11 (2009) 95–98.
[4] F. Zhou, M. Cococcioni, K. Kang, G. Ceder, Electrochem. Commun. 6 (2004) 1144–1148.
[5] D.Y. Wang, H. Buqa, M. Crouzet, G. Deghenghi, T. Drezen, I. Exnar, N.-H. Kwon, J.H. Miners, L. Poletto, M. Grätzel, J. Power Sources 189 (2009) 624–628.
[6] J. Barker, M.Y. Saïdi, US Patent 5,871,866 (1999).
[7] J. Gaubicher, C. Wurm, G. Goward, C. Masquelier, L. Nazar, Chem. Mater. 12 (2000) 3240–3242.
[8] H. Huang, S.C. Yin, T. Kerr, N. Taylor, L.F. Nazar, Adv. Mater. 14 (2002) 1525–1528.
[9] S.C. Yin, H. Grondey, P. Strobel, M. Anne, L.F. Nazar, J. Am. Chem. Soc. 125 (2003) 10402–10411.
[10] M.M. Ren, Z. Zhou, X.P. Gao, W.X. Peng, J.P. Wei, J. Phys. Chem. C 112 (2008) 5689–5693.
[11] H. Huang, T. Faulkner, J. Barker, M.Y. Saïdi, J. Power Sources 189 (2009) 748–751.
[12] L. Wang, L.C. Zhang, I. Lieberwirth, H.W. Xu, C.H. Chen, Electrochem. Commun. 12 (2010) 52–55.
[13] M.Y. Saïdi, J. Barker, H. Huang, J.L. Swoyer, G. Adamson, J. Power Sources 119–121 (2003) 266–272.
[14] S.Y. Chung, J.T. Bloking, Y.M. Chiang, Nat. Mater. 1 (2002) 123–128.
[15] S.C. Yin, P.S. Strobel, H. Grondey, L.F. Nazar, Chem. Mater. 16 (2004) 1456–1465.
[16] M. Sato, H. Ohkawa, K. Yoshida, M. Saito, K. Uematsu, K. Toda, Solid State Ionics 135 (2000) 137–142.
[17] D. Morgan, G. Ceder, M.Y. Saïdi, J. Barker, J. Swoyer, H. Huang, G. Adamson, Chem. Mater. 14 (2002) 4684–4693.
[18] M.M. Ren, Z. Zhou, Y.Z. Li, X.P. Gao, J. Yan, J. Power Sources 162 (2006) 1357–1362.
[19] J. Barker, R.K.B. Gover, P. Burns, A. Bryan, J. Electrochem. Soc. 154 (2007) A307–A313.
[20] Y.H. Chen, Y.M. Zhao, X.N. An, J.M. Liu, Y.Z. Dong, L. Chen, Electrochim. Acta 54 (2009) 5844–5850.
[21] Q. Kuang, Y.M. Zhao, X.N. An, J.M. Liu, Y.Z. Dong, L. Chen, Electrochim. Acta 55 (2010) 1575–1581.
[22] J. Barker, M.Y. Saïdi, J.L. Swoyer, Electrochem. Solid-State Lett. 6 (2003) A53–A55.
[23] D.Y. Wang, H. Li, S.Q. Shi, X.J. Huang, L.Q. Chen, Electrochim. Acta 50 (2005) 2955–2958.
[24] Z. Sun, X. Shi, X. Wang, Y. Sun, Diamond Relat. Mater. 8 (1999) 1107–1113.
[25] B.J. Hwang, K.F. Hsu, S.K. Hu, M.Y. Cheng, T.C. Chou, S.Y. Tsay, R. Santhanam, J. Power Sources 194 (2009) 515–519.
[26] M.V. Reddy, G.V. Subba Rao, B.V.R. Chowdari, J. Phys. Chem. C 111 (2007) 11712–11720.
[27] X.C. Zhou, Y.M. Liu, Y.L. Guo, Electrochim. Acta 54 (2009) 2253–2258.
[28] Z. Zhou, J. Yan, Y.X. Li, D.Y. Song, Y.S. Zhang, J. Power Sources 72 (1998) 236–238.
[29] J. Kawakita, K. Makino, Y. Katayama, T. Miura, T. Kishi, J. Power Sources 75 (1998) 244–250.
[30] Y.P. Wu, E. Rahm, R. Holze, Electrochim. Acta 47 (2002) 3491–3507.